Molecular MRI enables early and sensitive detection of brain metastases

Sébastien Serres[a], Manuel Sarmiento Soto[a], Alastair Hamilton[a,b], Martina A. McAteer[c], W. Shawn Carbonell[a,d], Matthew D. Robson[e], Olaf Ansorge[f], Alexandre Khrapitchev[a], Claire Bristow[a], Lukxmi Balathasan[a], Thomas Weissensteiner[a], Daniel C. Anthony[b], Robin P. Choudhury[c], Ruth J. Muschel[a], and Nicola R. Sibson[a,1]

[a]CR-UK/MRC Gray Institute for Radiation Oncology and Biology, Department of Oncology, University of Oxford, Oxford OX3 7LJ, United Kingdom; [b]Department of Pharmacology, University of Oxford, Oxford OX1 3QT, United Kingdom; [c]Department of Cardiovascular Medicine, University of Oxford, John Radcliffe Hospital, Oxford OX3 9DU, United Kingdom; [d]Department of Neurological Surgery, University of California, San Francisco, CA 94158; [e]Oxford Centre for Clinical Magnetic Resonance Research, Department of Cardiovascular Medicine, University of Oxford, John Radcliffe Hospital, Oxford OX3 9DU, United Kingdom; and [f]Department of Clinical Neuropathology, John Radcliffe Hospital, Oxford OX3 9DU, United Kingdom

Edited by Erkki Ruoslahti, Sanford–Burnham Medical Research Institute at University of California, Santa Barbara, CA, and approved March 2, 2012 (received for review October 24, 2011)

Metastasis to the brain is a leading cause of cancer mortality. The current diagnostic method of gadolinium-enhanced MRI is sensitive only to larger tumors, when therapeutic options are limited. Earlier detection of brain metastases is critical for improved treatment. We have developed a targeted MRI contrast agent based on microparticles of iron oxide that enables imaging of endothelial vascular cell adhesion molecule-1 (VCAM-1). Our objectives here were to determine whether VCAM-1 is up-regulated on vessels associated with brain metastases, and if so, whether VCAM-1–targeted MRI enables early detection of these tumors. Early up-regulation of cerebrovascular VCAM-1 expression was evident on tumor-associated vessels in two separate murine models of brain metastasis. Metastases were detectable in vivo using VCAM-1–targeted MRI 5 d after induction (<1,000 cells). At clinical imaging resolutions, this finding is likely to translate to detection at tumor volumes two to three orders of magnitude smaller (0.3–3 × 10^5 cells) than those volumes detectable clinically (10^7–10^8 cells). VCAM-1 expression detected by MRI increased significantly ($P < 0.0001$) with tumor progression, and tumors showed no gadolinium enhancement. Importantly, expression of VCAM-1 was shown in human brain tissue containing both established metastases and micrometastases. Translation of this approach to the clinic could increase therapeutic options and change clinical management in a substantial number of cancer patients.

Metastasis, the spread of cancer from the primary tumor site to distant organs, remains one of the greatest hurdles in cancer therapy, and it is a leading cause of cancer mortality. Metastases represent the most common cancer in the brain, outnumbering primary brain tumors 10-fold, and 20–40% of all cancer patients will develop metastatic spread to the brain (1). Clinically, brain metastases are diagnosed only when they are sufficiently large to be detected with imaging and prognosis is poor (2). MRI is being used increasingly to detect brain metastases, and it has shown a significant increase in sensitivity over both computed tomography (CT) alone (3, 4) and PET/CT (5) for detection of small or asymptomatic metastases. However, the gold standard MRI technique of passive contrast enhancement relies on blood–brain barrier (BBB) breakdown, an approach that is more sensitive to later-stage metastases. Survival is typically of the order of a few months, even with treatment, most likely owing to the late stage of diagnosis. For patients with primary lung or breast cancer at high risk of brain metastasis, prophylactic whole-brain radiotherapy (WBRT) may be used to eliminate potential occult micrometastases. However, WBRT itself is associated with substantive adverse neurological effects and may be unnecessary in a significant number of patients. It has become clear, therefore, that one of the major limiting factors in the treatment of brain metastases is our inability to detect them early enough for therapy to be both appropriately prescribed and maximally effective. However, the potential benefit of earlier treatment will remain a hypothesis until diagnostic methods are developed that enable such a window of opportunity to be opened. Thus, the development of new methods for detecting the early stages of metastatic disease in the brain is critical.

The vascular endothelium of the brain plays an essential role in the maintenance of the brain microenvironment, and its functional phenotype is dynamically responsive to pathological stimuli. Many of the functions of the vascular endothelium are mediated by surface molecules, such as cell adhesion molecules (CAMs). These CAMs can be rapidly up-regulated in response to disease or injury, and they mediate leukocyte rolling, adhesion, and transmigration across the BBB (6). In particular, vascular cell adhesion molecule-1 (VCAM-1) has been shown to play an important role in leukocyte recruitment to the brain in neurological disease both in animal models and humans (7–10). We and others have previously shown a close association of tumor colonies with the existing cerebral vasculature both in murine models of brain metastasis and human postmortem brain tissue containing metastases (11, 12). These findings suggest that activation of the vascular endothelium is likely to occur during metastasis development. Moreover, there is evidence to suggest that tumor cells use inducible CAMs to promote their adhesion to the vascular endothelium, and both VCAM-1 and E/P-selectin have been found to be up-regulated in lung and liver metastases (13–16). Based on these findings, we hypothesized that local up-regulation of VCAM-1 may occur in the very early stages of metastasis in the brain.

MRI has proved effective for both in vivo cell tracking and detection of molecular processes through the use of contrast agents comprised of microparticles of iron oxide (MPIO). These agents provide high sensitivity contrast owing to their potent superparamagnetic properties. This property has previously been used to track MPIO-labeled tumor cells in mouse models, thus enabling visualization of early metastasis distribution in the brain with sensitivity down to a single metastatic cell loaded with ~50 pg iron at an imaging field strength of 1.5 T (17). Alternatively, conjugation of MPIO with targeting ligands enables their accumulation at sites where specific molecules are expressed (18–25). Importantly, the targeted MPIO are not taken up by endothelial cells and do not enter the brain, thus providing an endovascular biomarker for pathology within the brain. In particular, we have shown that, by conjugating anti–VCAM-1 antibodies to MPIO, we are able to detect VCAM-1 up-regulation on the cerebral endothelium with high sensitivity in vivo (19). Our objectives, therefore, were to determine whether endothelial VCAM-1 is up-regulated in association with brain metastases, and if so, whether our

Author contributions: S.S., D.C.A., R.P.C., R.J.M., and N.R.S. designed research; S.S., M.S.S., A.H., W.S.C., M.D.R., O.A., A.K., C.B., L.B., T.W., D.C.A., and N.R.S. performed research; M.A.M., M.D.R., and R.P.C. contributed new reagents/analytic tools; S.S., M.S.S., A.H., M.D.R., and N.R.S. analyzed data; and S.S., M.S.S., A.H., M.D.R., and N.R.S. wrote the paper.

The authors declare no conflict of interest.

This article is a PNAS Direct Submission.

[1]To whom correspondence should be addressed. E-mail: nicola.sibson@oncology.ox.ac.uk.

This article contains supporting information online at www.pnas.org/lookup/suppl/doi:10.1073/pnas.1117412109/-/DCSupplemental.

VCAM-1–targeted MRI contrast agent could enable early detection of these tumors.

Results

No clinical signs were evident in any of the groups injected with 4T1 cells or in three out of four of the MDA231BR-injected mice; in the fourth animal, hind limb paralysis became apparent at day 20. Metastases were detected in the brains of all mice injected with 4T1 cells (Fig. 1). The area encompassed by tumors at day 5 was considerably smaller than at days 10 and 13, and their location was predominantly intravascular (Fig. 1*A*). By day 10, the tumor colonies were mostly found on the parenchymal side of the vascular endothelium (Fig. 1*B*), and expansion occurred along the cerebral blood vessels between days 10 and 13 (Fig. 1*C*). Metastases were distributed throughout the brain, with greater numbers found in the cerebellum, olfactory bulbs, and around the dentate gyrus. Strong endothelial VCAM-1 expression in 4T1-injected mice was shown immunohistochemically (Fig. 1*D*) and frequently colocalized with metastases. Occasionally, VCAM-1 expression was observed in the absence of histologically detectable tumors. Colocalization of VCAM-1 and tumor colonies was confirmed by immunofluorescence; Fig. 1*E* shows the close association of VCAM-1–positive vessels (red) with a metastasis (green) at day 10, while Fig. 1*F* shows the spatial spread of VCAM-1 around a metastasis at day 13 encompassing endothelial and some glial expression.

In Vivo Detection of VCAM-1 Up-Regulation by MRI. VCAM–MPIO caused a marked MRI contrast effect evident as focal hypointense areas on T_2*-weighted images throughout the forebrain, olfactory bulbs, and cerebellum (Figs. 1*G* and 2). Spatial correspondence of MRI-detectable hypointensities with brain metastases detected immunohistochemically was clearly evident in some cases (Fig. 1 *G–I*), although differences in spatial resolution between the two approaches and partial volume effects in the MRI data limit such assessment. Bound VCAM–MPIO were observed histologically in vessels either within or closely associated with tumor colonies (Fig. 1 *A–C*, *Insets*). VCAM–MPIO-induced hypointensities were observed in 4T1-injected mice from the earliest time point studied, day 5, and increased markedly over time (Fig. 2 *A–C*). Little or no MPIO retention was detected in naïve animals injected with VCAM–MPIO (Fig. 2*D*) or 4T1-injected mice administered with the control contrast agent, IgG–MPIO.

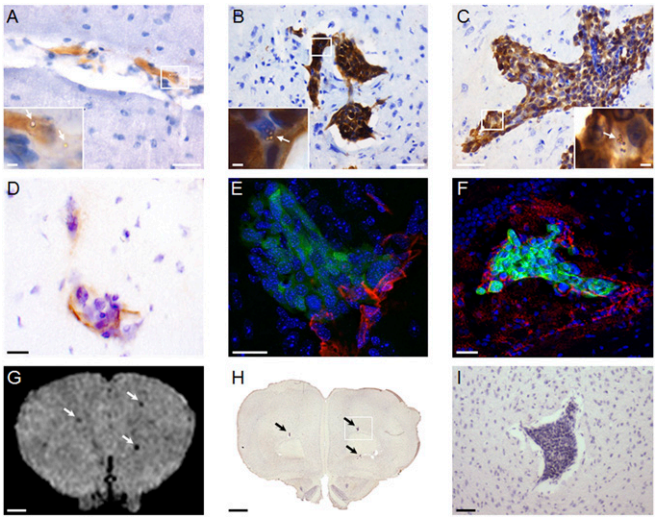

Fig. 1. Immunohistochemical detection of brain metastases in 4T1 model. (*A–C*) Photomicrographs of tumor colonies at days 5 (*A*), 10 (*B*), and 13 (*C*) after 4T1 injection. (Scale bars: 100 μm.) *Insets* show magnified regions of the tumors with endothelial binding of VCAM–MPIO (arrows). (Scale bars: 20 μm.) (*D*) Immunohistochemical colocalization of VCAM-1 (brown) with a brain metastasis at day 10. (*E* and *F*) Colocalization of VCAM-1 (red) with GFP-positive tumors (green) detected by confocal microscopy at days 10 and 13, respectively. Cell nuclei are stained blue. (Scale bars: *D–F*, 10 μm.) (*G–I*) Colocalization of focal hypointensities on a T2*-weighted image (*G*; arrows) with histological detection of metastases (*H*; arrows). (*I*) Zoomed view of the box indicated in *H*. (Scale bars: *G* and *H*, 1 mm; *I*, 100 μm.)

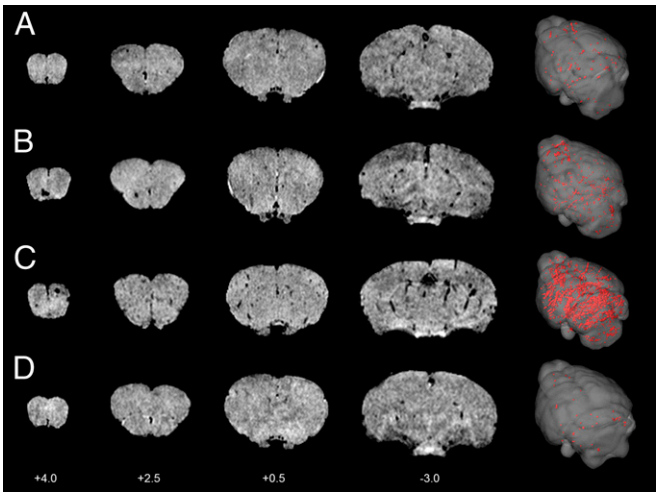

Fig. 2. MRI detection of VCAM–MPIO binding in 4T1 model. Selected T_2*-weighted images from a 3D dataset (coordinates relative to Bregma) at days 5 (*A*), 10 (*B*), and 13 (*C*) after intracardiac injection of 4T1 cells. Intense focal hypointense areas (black) correspond to MPIO binding. No specific MPIO binding was detected in naïve BALB/c mice injected with VCAM–MPIO (*D*). 3D reconstructions (column 5) show the spatial distribution of VCAM–MPIO binding (red) throughout the brain.

Quantitation of MRI and Immunohistochemistry Data. The volume of hypointensities on T2*-weighted images in VCAM–MPIO-injected animals increased significantly over time ($P < 0.0001$) (Fig. 3*A*). VCAM–MPIO binding in 4T1-injected animals was significantly greater at all time points than the binding measured in naïve mice (day 5: $P < 0.01$, day 10: $P < 0.0001$, day 13: $P < 0.001$) (Fig. 3*A*). Similarly, the volume of VCAM–MPIO-induced hypointensities at day 10 was significantly greater than the volume measured in IgG–MPIO-injected mice at day 10 ($P < 0.0001$) (Fig. 3*A*). VCAM–MPIO binding in 4T1-injected animals increased approximately sevenfold between days 5 and 13 and was significantly greater at day 13 than both days 5 and 10 ($P < 0.001$) (Fig. 3*A*). No significant difference was found between the volumes of hypointensity observed in 4T1-injected mice given IgG–MPIO and naïve mice injected with VCAM–MPIO.

Few metastases were detectable at day 5 immunohistochemically, but this increased over time (Fig. 3*B*). Similarly, the mean tumor area (per millimeter squared brain area) at day 5 was very small, but it increased significantly over time ($P < 0.05$) and was significantly greater at both days 10 and 13 than day 5 ($P < 0.05$) (Fig. 3*C*). Positive correlations were found between both the number and area of tumor colonies (per millimeter squared brain area) and the volume of MRI-detectable hypointensities ($P < 0.05$) (Fig. 3 *E* and *F*). Assessment of tumor colocalization with MRI-detectable hypointensities at day 10 indicated that, as the tumor volume (assessed histologically) increased, the likelihood of MRI detection increased; therefore, above the mean tumor size, 68% of tumors were positively identified by MRI, whereas below the mean, only 36% were successfully identified (Fig. 3*D*). Similarly, immunofluorescence analysis showed that, above the mean tumor size, 65% of tumors were VCAM-1–positive, whereas below the mean, 43% were VCAM-1–positive (Fig. 3*D*). At this time, the average tumor size was ~760 cells, whereas the average metastasis positively correlated with both MRI and VCAM-1 expression was ~1,300 cells; the smallest positively correlated tumor was ~30 cells.

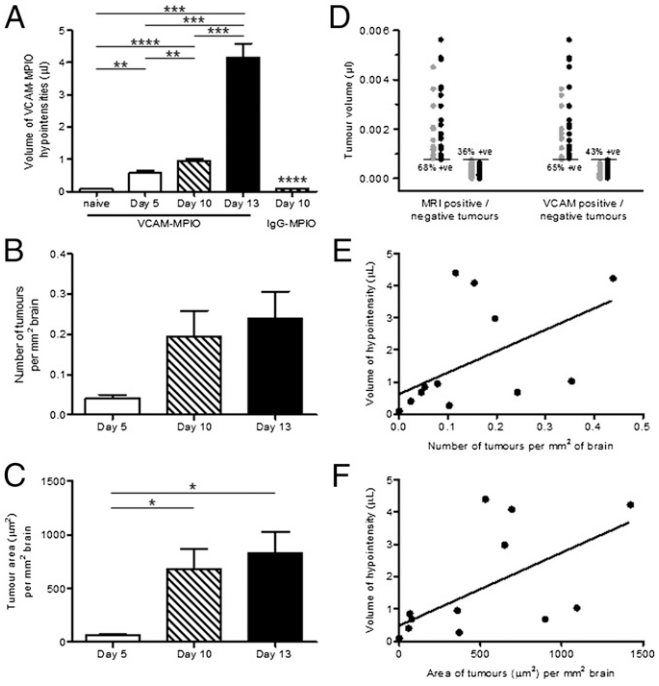

Fig. 3. Quantitation of VCAM–MPIO binding and tumor number/area in 4T1 model. (*A*) The volume of hypointensities on T2*-weighted images in VCAM–MPIO-injected animals increased significantly over time (n = 5–6 per group). Significance shown for the day 10 IgG–MPIO group is compared with the day 10 VCAM–MPIO group. (*B* and *C*) Graphs to show change in number (*B*) and area (*C*) of tumor colonies over time after intracardiac 4T1 cell injection (n = 3 on day 5; n = 4 on days 10 and 13). (*D*) Graph indicating volumes of metastases at day 10 that were MRI- or VCAM-1–positive (black circles) and MRI- or VCAM-1–negative (gray circles). Percentages of positive values (MRI or VCAM-1) are given for cohorts of tumors above and below the mean tumor volume (horizontal lines). Correlation analysis between the volume of hypointensities on T2*-weighted images and the number (*E*) or area (*F*) of tumor colonies revealed significant positive correlations ($P < 0.05$; r^2 = 0.3 and 0.4, respectively). In all cases, *$P < 0.05$, **$P < 0.01$, ***$P < 0.001$, and ****$P < 0.0001$.

VCAM-1 Expression in MDA231BR Brain Metastasis. At day 21 in the MDA231BR-injected mice, the mean tumor area (548 ± 117 µm^2/mm^2 brain) was similar to the area measured at day 10 in the 4T1 model (680 ± 187 µm^2/mm^2 brain). Again, binding of VCAM–MPIO was evident as focal hypointense areas on T_2*-weighted images throughout the brain (Fig. 4). Colocalization of the MRI-detectable hypointensities with immunohistochemical detection of both tumor colonies and VCAM-1 expression was evident (Fig. 4 *B*, *C*, and *C1–C4*). Quantitatively, the volumes of VCAM–MPIO-induced hypointensities in these animals lay between those volumes found at days 10 and 13 in the 4T1 model (1.92 ± 0.65 vs. 0.96 ± 0.04 and 4.16 ± 0.43 µL, respectively).

Comparison with Clinically Used Gd-DTPA Enhancement. No gadolinium-DTPA (Gd-DTPA) enhancement was found on T_1-weighted images acquired from any of the 4T1-injected mice, indicating a lack of BBB breakdown (Fig. S1). Similarly, no evidence of BBB breakdown was found in three out of four of the MDA231BR-injected animals (Fig. S1). In the fourth animal, which showed clinical symptoms at day 20, a single area of Gd-DTPA enhancement was found in the left motor cortex. Intense VCAM–MPIO contrast was also evident in this region but spatially distinct, indicating that the VCAM–MPIO were still endovascularly bound, whereas the Gd-DTPA had extravasated into the parenchyma (Fig. S2). In this animal, other areas of VCAM–MPIO contrast were also evident elsewhere in the brain, with no concomitant Gd-DTPA enhancement (Fig. S2). The dose of Gd-DTPA used in all of the above experiments was approximately six times the lowest clinical dose. Three animals injected intracardially with 4T1 cells were also imaged pre- and post–Gd-DTPA at a clinically relevant dose (57.4 mg/kg) on day 10. As with the higher Gd-DTPA dose, none of these animals showed any evidence of BBB breakdown (Fig. S3).

VCAM-1 Expression in Human Brain Metastasis Tissue. Strong endothelial VCAM-1 staining was confirmed in a control brain sample with nonspecific inflammation (Fig. 5*A*), whereas immunoreactivity was barely visible in control brains (Fig. 5*B*). The majority of the tumor samples studied were from fully established metastases of surgical material, where diagnosis had been confirmed by CT or contrast-enhanced MRI. VCAM-1 was variably expressed on the endothelial cells of solid metastases (Fig. 5 *C–E*), and expression was strongest when the metastases elicited a marked inflammatory response (Fig. 5*E*). One metastasis also showed strong staining of the tumor cell membranes (Fig. 5*D*). Although it is difficult to obtain tissue from early-stage brain metastases, because these metastases cannot be diagnosed, we were able to find a few such samples. The best cases were those cases with carcinomatous meningitis, where individual cell clusters that were invading the brain parenchyma along perivascular spaces could be identified. Importantly, in these samples, strong VCAM-1 expression was found in vessels adjacent to micrometastases consisting of just a monolayer of perivascular cells or small perivascular cell clusters (Fig. 5 *F* and *G*). Vessels remote from the metastatic deposit in the same section showed no significant immunoreactivity.

Discussion

In this study, we have shown close association of brain metastases with the vasculature over the early stages of development. Acute activation of the vascular endothelium within and around the tumors was also evident from an early time point with marked VCAM-1 expression. We have shown that, through the use of a targeted contrast agent that binds to VCAM-1, it is possible to detect metastases in the brain using MRI substantially earlier than is possible with the clinically used approach of passive gadolinium enhancement. Expression of VCAM-1 and VCAM–MPIO binding increased rapidly with tumor growth, indicating sensitivity to disease progression. We have also shown that there is increased expression of VCAM-1 on the vascular endothelium within and around metastases in human brain tissue and even in vessels associated with only a monolayer of perivascular tumor cell. Thus, we believe that this approach may provide a highly sensitive method for the early detection of brain metastases clinically.

VCAM-1 Up-Regulation in Murine Models of Brain Metastasis. The ability of cells to metastasize from a primary tumor to a distant site requires several properties, of which one is the capacity to adhere to the endothelium in specific vascular beds. Although it has been suggested that tumor cells may exploit the same mechanisms used by leukocytes for adhesion to and extravasations across the vascular endothelium (26), it remains unclear which specific ligands are responsible for this process. In a melanoma model, both blockade and inhibition of VCAM-1 have been shown to significantly reduce liver metastasis (16, 27). Similarly, disruption of the interaction between very late antigen-4, the natural ligand to VCAM-1, on tumor cells and endothelial VCAM-1 reduces both adhesion of metastatic renal cell cancer cells to endothelial cells in vitro (28) and incidence of lung metastases in vivo (29). Moreover, several human tumor cell lines that metastasize to the lung show greater expression of very late antigen-4 than non-metastatic lines (30). Thus, it has been suggested that adhesion molecules, including VCAM-1, play an important role in both initiating adhesion events in metastasis and facilitating colony progression (31). Despite the above findings, very little data exists with respect to the up-regulation of adhesion molecules in brain metastasis. In one study, up-regulation of VCAM-1 was found in the brains of mice with heavy pulmonary metastasis burden, and 25% of these mice had evidence of brain metastases (32).

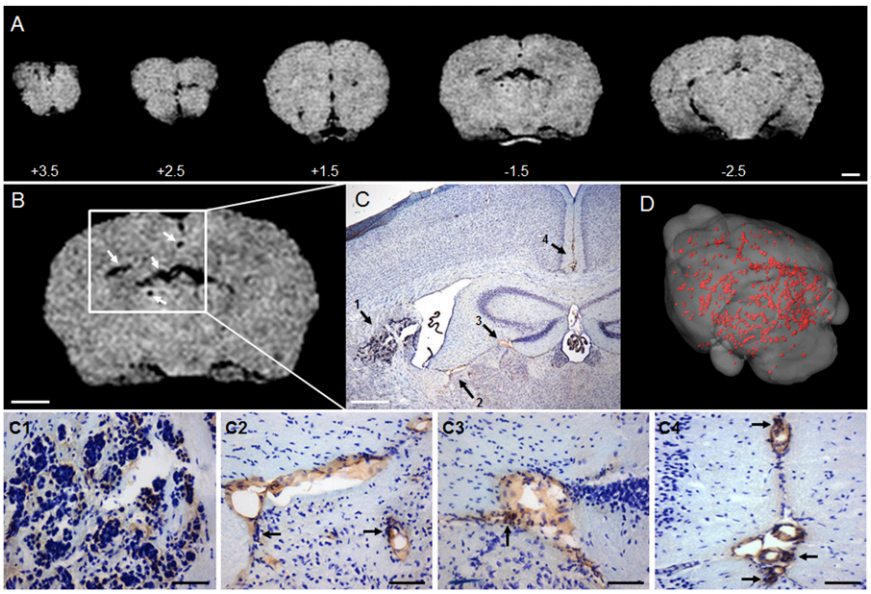

Fig. 4. VCAM–MPIO binding and tumor detection in the MDA231BR model. (*A*) Selected T_2*-weighted images from a 3D dataset (coordinates relative to Bregma) at day 21 after intracardiac injection of MDA231BR cells. Intense focal hypointense areas (black) correspond to VCAM–MPIO binding (Scale bar: 1 mm.) (*B* and *C*) Colocalization of the MRI hypointense signals (arrows) with VCAM-1 expression (brown) and metastases (arrows). *C1–C4* show higher magnification photomicrographs of the four tumor colonies highlighted in *C*. (Scale bars: *B*, 1 mm; *C*, 200 μm; *C1–C4*, 50 μm.) (*D*) 3D reconstruction shows the spatial distribution of VCAM–MPIO binding (red).

However, colocalization of VCAM-1 expression with brain metastases was not shown, and it was not possible to conclude from that study whether brain VCAM-1 up-regulation was a result of the systemic disease burden and increased circulating cytokine levels or brain metastases per se. Here, we have shown that there is acute up-regulation of VCAM-1 on the cerebral vasculature in association with brain metastases and that this expression increases with tumor colony expansion. These data suggest that VCAM-1 may play a role in the establishment and progression of brain metastases.

VCAM-1–Targeted MRI Detection of Brain Metastases. We have shown that the use of VCAM–MPIO in conjunction with MRI enables detection of brain metastases early in their development. The increase in binding of VCAM–MPIO observed with tumor colony expansion in the 4T1 model indicates the responsiveness of this biomarker to disease progression, whereas the detection of tumors as early as day 5 indicates sensitivity to even very small micrometastases. At all time points studied in the 4T1 model, no evidence of post–Gd-DTPA contrast enhancement was evident on T1-weighted images, which is the current clinical gold standard for brain metastasis detection. Other studies of brain metastasis models in mice have indicated that breakdown of the BBB does not occur until tumors are >500 μm in diameter, which is considerably larger than those tumors found at any time point studied here (maximum diameter of ∼100 μm). The current limit of detection clinically for brain metastases is 2–5 mm when the BBB becomes permeable (33), although they are more typically detected between 5 mm and 1 cm in diameter (34). In the 4T1-injected mice, the average MRI-detectable tumor observed at day 10 comprised $\sim 1 \times 10^3$ cells, which is approximately four orders of magnitude smaller than the approximate size, 1×10^7 cells, of a 2-mm diameter metastasis in human brain. It should be noted that the spatial resolution achievable in mice is considerably higher than the resolution that is possible clinically, and as voxel sizes increase, the number of VCAM–MPIO per voxel must be higher to induce a detectable contrast change. We have estimated, based on the detection limits observed in the current study and common clinical resolutions at 3 T, that metastases of the order of 300–650 μm in diameter ($\sim 0.3–3 \times 10^5$ cells) should be detectable clinically

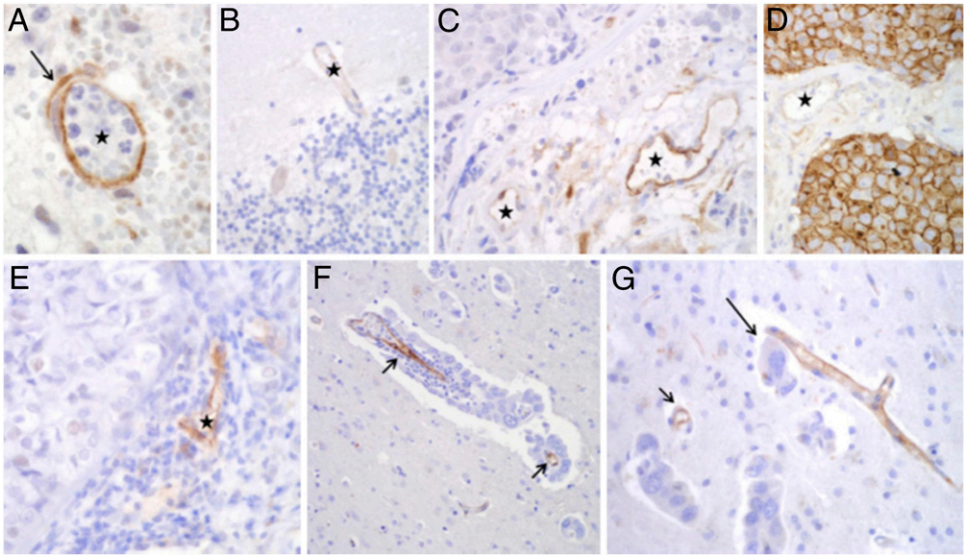

Fig. 5. VCAM-1 expression in human brain metastasis. (*A*) Positive control section showing VCAM-1 expression (brown) on a brain vessel (★) adjacent to acute inflammation. (*B*) Normal brain tissue showing minimal VCAM-1 reaction in cortical vessel (★). (*C*) Strong VCAM-1 staining in stromal endothelial cells of a metastatic carcinoma (★); solid carcinoma is in the upper left corner. (*D*) In one case, VCAM-1 staining was evident on the membranes of the carcinoma cells themselves as well as on stromal vessels (★). (*E*) Substantial endothelial VCAM-1 expression in a stromal vessel of a metastasis that evoked chronic inflammation (★). (*F* and *G*) Selective expression of VCAM-1 by endothelial cells in close proximity to perivascular brain micrometastases (arrows). Note intimate association of three tumor cells (*G*; long arrow) with a VCAM-1–positive small vessel. (Magnification: *A–F*, 400×; *G*; 200×.)

(*SI Text 1*). We have also measured the attainable signal to noise on a 3-T human scanner at 1 mm isotropic resolution and a scan time of 9.5 min, and we have shown that it is sufficient to observe the estimated signal change (*SI Text 1* and Fig. S4). These estimates indicate that, at the resolution limits permitted by clinical MRI scanners, brain metastases will still be detectable considerably earlier using VCAM-targeted MRI than is currently possible. With the advent of higher-field human scanners (7 T) and more sensitive susceptibility-weighted imaging and steady-state free precession sequences, this detection sensitivity should improve further (35, 36).

Although not all tumors seemed to be colocalized with either MRI-detectable hypointensities or detectable VCAM-1 expression, in both cases, this colocalization increased with increasing tumor volume. It is likely that some, at least, of these apparent false negatives arise from difficulties in coregistering two modalities with very different spatial resolution. Thus, although an estimate only, these numbers indicate that, as the metastases grow, they become more readily detectable. As might be expected, quantitatively, the VCAM–MPIO volumes of hypointensity correlated more closely with tumor area than number, reflecting greater endothelial activation with tumor expansion. Moreover, below the average tumor size at day 10 (Fig. 3*D*), considerably fewer tumors were VCAM-1–positive, suggesting that the metastases must reach a certain size or stage of development to induce sufficient VCAM-1 for effective VCAM–MPIO binding. Shapiro et al. (37) have previously shown that, at similar resolutions to this study, single 1-μm MPIO are readily detectable. Extrapolating from that study, tumors in which one or more VCAM–MPIO had bound are likely to have been detectable here.

Interestingly, the findings from the anomalous MDA231BR-injected mouse showing a single area of Gd-DTPA enhancement indicate that, even when clinical symptoms and Gd-detectable metastases become apparent, the VCAM–MPIO approach reveals additional tumor burden that remains undetectable by conventional means. Thus, even at later stages, VCAM-targeted MRI is likely to provide a more accurate measure of tumor burden than current methods. The disproportionate increase in VCAM-1 expression (VCAM–MPIO binding) compared with tumor growth between days 10 and 13 may reflect, in part, a greater spatial spread of VCAM-1 expression through cascading activation of the vascular endothelium. Such spreading endothelial activation may also explain the occasional observation of apparently nontumor-related VCAM-1 expression. At the same time, it has been shown in vitro that leukocytes binding to the endothelium can induce the formation of transmigratory cups on endothelial cells comprised of numerous vertical microvilli-like projections rich in VCAM-1 (38). Thus, the greater binding of VCAM–MPIO at day 13 may also reflect an increase in VCAM-1 expression and presentation on endothelial cells owing to leukocyte and/or tumor cell binding.

The low background or nonspecific MPIO binding in the control groups indicates both the high specificity of the VCAM–MPIO for VCAM-1 expression, as previously shown (19), and the lack of constitutive VCAM-1 expression in normal cerebral vasculature. This latter finding is in accord with our previous findings and suggests that up-regulation of VCAM-1 is a consequence rather than an initiating event for the development of brain metastases. Furthermore, the low background signal observed in the control groups illustrates one of the major advantages of the micrometer-sized iron oxide particles used here: their very rapid clearance from the circulation, which enables detection of specific binding contrast rapidly after contrast agent injection. Importantly, at clinical imaging resolutions, these nonspecific hypointensities will be undetectable (*SI Text 1*), and thus, the false-positive rate from nonspecific MPIO retention should be zero clinically.

Relevance to Human Brain Metastasis. Up-regulation of VCAM-1 expression was evident in all of the samples of human brain tissue containing metastases that were studied, with no evidence of significant constitutive expression in control brain tissue. The degree of VCAM-1 expression seemed to be greater when an overt inflammatory response was evident. Importantly, as for the murine models, VCAM-1 up-regulation also seems to occur early in human brain metastasis, with expression being evident in vessels associated with just a monolayer of perivascular tumor cells. These data strongly support the application of our VCAM–MPIO approach as a diagnostic tool for the early detection of brain metastases in man.

The MPIO used in this proof of concept study were nonbiodegradable and are not suitable for use in humans. However, iron oxide-containing contrast media are in clinical use (39, 40), and both we and others (41) are developing micrometer-sized biodegradable particles. Smaller iron oxide particles, such as superparamagnetic particles of iron oxide (SPIO) and ultrasmall SPIO (USPIO), cannot be used for this application owing, in part, to their long half-life (42), which precludes rapid molecular imaging of target-specific binding because of high background levels. At the same time, considerably greater numbers of USPIO/SPIO are required to achieve the same contrast effect as for MPIO because of the markedly lower iron content and greatly reduced targeting valency of each particle [USPIO = 2.4–24 antibodies per particle (43) vs. VCAM–MPIO ~ 25,000 antibodies per particle]. To date, no adverse events with the nonbiodegradable VCAM–MPIO have been observed in mice over 72 h after administration, and we have previously reported that, at both 30 min and 24 h after administration, antibody-conjugated 1-μm MPIO accumulate predominantly in the spleen and liver (24, 44). We have now also assessed the possibility of systemic macrophage activation at the molecular level as a consequence of VCAM–MPIO administration, and we have found that an antiinflammatory rather than proinflammatory phenotype is induced in the liver (*SI Text 2* and Fig. S5).

One potential issue with the VCAM–MPIO/MRI approach is that nontumor-associated inflammation could lead to false positives. However, several factors would minimize the likelihood of this finding, including (*i*) screening of only the subset of patients at risk for brain metastasis and (*ii*) the spatial information inherent in MRI data—clinically, brain metastases are most commonly located at the gray-white matter junction and terminal watershed zones of the cerebral hemispheres, whereas nonspecific inflammation is likely to be more widespread; also, the archetypal inflammatory disease of the brain, multiple sclerosis, commonly presents within the white matter tracts, cerebellum, and brainstem. Moreover, the current clinical diagnostic test for brain metastases, passive gadolinium-based contrast enhancement, is not specific to brain metastasis and as shown here, is considerably less sensitive than VCAM-targeted MRI with respect to both early detection and evaluation of full tumor burden.

Brain metastasis remains a challenging clinical problem. As our ability to detect and treat primary and systemic metastatic disease improves, effective treatment of brain metastases is becoming increasingly urgent. Earlier detection is likely to yield substantial gains for both the application of current therapies and the development of new metastasis-inhibiting agents. Most potential therapies fail to show their efficacy endpoints in phase III trials or earlier, in part owing to the late stage of tumor diagnosis. Earlier diagnosis through the use of this VCAM-1–targeted MRI approach could open a window of therapeutic opportunity that currently does not exist in brain metastasis and guide decisions on treatment options. Moreover, more sensitive monitoring of disease burden may be beneficial in the assessment of new therapies and allow earlier decisions to be made on efficacy.

Methods

Experimental Models. Seven- to eight-week-old female BALB/c mice (n = 19) were anesthetized with 2–3% isoflurane in O_2 and injected in the left ventricle of the heart with 1×10^5 4T1 (metastatic murine mammary carcinoma) (45) cells in 100 μL PBS. Mice were recovered from anesthesia and underwent MRI at day 5, 10, or 13 after 4T1 cell injection. Seven- to eight-week-old female SCID mice (n = 4) were anesthetized and injected intracardially as above with 1×10^5 MDA231BR (subclone of metastatic human breast carcinoma that preferentially metastasizes to the brain) (46) cells in 100 μL PBS. Mice underwent MRI 21 d after intracardiac injection, because these tumors are slower-growing than the 4T1 metastases. All experiments were approved by the UK Home Office.

Experimental Protocol. VCAM–MPIO or control IgG–MPIO were synthesized as described previously (19). On the day of imaging, 4T1-injected mice were anesthetized with 2–3% (vol/vol) isoflurane in 70% N_2O:30% O_2 (vol/vol) and injected i.v. through a tail vein with VCAM–MPIO (4 mg Fe/kg body weight in 100 μL saline; n = 5–6 per time point). A separate group of mice at day 10 post-4T1 cell injection were injected i.v. with IgG–MPIO (4 mg Fe/kg body weight in 100 μL saline; n = 3). Another cohort of naïve BALB/c mice was injected i.v. with VCAM–MPIO as above (n = 3). MDA231BR-injected animals were anesthetized and injected i.v. with VCAM–MPIO as above (n = 4). Mice were allowed to recover from anesthesia for 30 min; they were then reanesthetized with 1–2% (vol/vol) isoflurane in 70% N_2O:30% O_2 (vol/vol) and positioned in a quadrature birdcage coil (2.6 cm internal diameter; RAPID MR International). ECG was monitored, and body temperature was maintained at ∼0.37 °C.

Full details of MRI data acquisition and analysis are in *SI Text 3*. In brief, a 3D T_2*-weighted dataset followed by pre- and post–Gd-DTPA T_1-weighted images were acquired on a 7-T MRI system. T_2*-weighted data were masked, thresholded, and stacked into a single sequence in ImagePro (Media Cybernetic). MPIO binding, defined as all voxels with signal levels of zero, was quantified and expressed in microliters. After MRI, animals were transcardially perfusion-fixed for subsequent histological analysis. Full details of immunohistochemical and immunofluorescence methods and data analysis are given in *SI Text 3*. Data are given as mean tumor area or number per millimeter squared brain area for either n = 3 (day 5) or n = 4 (days 10 and 13). In 3 mice, at day 10 after 4T1 injection, spatial correlation between immunohistochemical and MRI detection of tumors as well as immunohistochemical colocalization of vascular VCAM-1 expression and tumor colonies were assessed as described in *SI Text 3*. All statistical tests are detailed in *SI Text 3*.

Immunohistochemistry of Human Tissue. Twelve cases of human brain metastasis together with one normal brain sample and one VCAM-1–positive control brain sample were examined immunohistochemically to assess VCAM-1 up-regulation (ethics reference 06/Q1604/141) as described in *SI Text 3*.

ACKNOWLEDGMENTS. The authors thank Nicky Sullivan and Yvonne Couch for technical help with the human immunohistochemistry and mouse tissue quantitative PCR, respectively. This work was funded by a Senior Fellowship from The Wellcome Trust (to R.P.C.), Cancer Research United Kingdom Grants C5255/A12678 (to R.J.M.) and C28461 (to N.R.S.), and the National Institute for Health Research Oxford Comprehensive Biomedical Research Centre and Nuffield Oxford Hospitals Fund.

1. Nussbaum ES, Djalilian HR, Cho KH, Hall WA (1996) Brain metastases. Histology, multiplicity, surgery, and survival. *Cancer* 78:1781–1788.
2. Weil RJ, Palmieri DC, Bronder JL, Stark AM, Steeg PS (2005) Breast cancer metastasis to the central nervous system. *Am J Pathol* 167:913–920.
3. Hochstenbag MM, Twijnstra A, Wilmink JT, Wouters EF, ten Velde GP (2000) Asymptomatic brain metastases (BM) in small cell lung cancer (SCLC): MR-imaging is useful at initial diagnosis. *J Neurooncol* 48:243–248.
4. Suzuki K, et al. (2004) Magnetic resonance imaging and computed tomography in the diagnoses of brain metastases of lung cancer. *Lung Cancer* 46:357–360.
5. Krüger S, et al. (2011) Brain metastasis in lung cancer. Comparison of cerebral MRI and 18F-FDG-PET/CT for diagnosis in the initial staging. *Nucl Med (Stuttg)* 50:101–106.
6. Ley K, Laudanna C, Cybulsky MI, Nourshargh S (2007) Getting to the site of inflammation: The leukocyte adhesion cascade updated. *Nat Rev Immunol* 7:678–689.
7. Cannella B, Raine CS (1995) The adhesion molecule and cytokine profile of multiple sclerosis lesions. *Ann Neurol* 37:424–435.
8. Piraino PS, et al. (2002) Prolonged reversal of chronic experimental allergic encephalomyelitis using a small molecule inhibitor of alpha4 integrin. *J Neuroimmunol* 131: 147–159.
9. Polman CH, et al. (2006) A randomized, placebo-controlled trial of natalizumab for relapsing multiple sclerosis. *N Engl J Med* 354:899–910.
10. Yednock TA, et al. (1992) Prevention of experimental autoimmune encephalomyelitis by antibodies against alpha 4 beta 1 integrin. *Nature* 356:63–66.
11. Carbonell WS, Ansorge O, Sibson N, Muschel R (2009) The vascular basement membrane as "soil" in brain metastasis. *PLoS One* 4:e5857.
12. Küsters B, et al. (2002) Vascular endothelial growth factor-A(165) induces progression of melanoma brain metastases without induction of sprouting angiogenesis. *Cancer Res* 62:341–345.
13. Läubli H, Borsig L (2010) Selectins as mediators of lung metastasis. *Cancer Microenviron* 3:97–105.
14. Ludwig RJ, et al. (2004) Endothelial P-selectin as a target of heparin action in experimental melanoma lung metastasis. *Cancer Res* 64:2743–2750.
15. Khatib AM, et al. (1999) Rapid induction of cytokine and E-selectin expression in the liver in response to metastatic tumor cells. *Cancer Res* 59:1356–1361.
16. Vidal-Vanaclocha F, et al. (2000) IL-18 regulates IL-1beta-dependent hepatic melanoma metastasis via vascular cell adhesion molecule-1. *Proc Natl Acad Sci USA* 97: 734–739.
17. Heyn C, et al. (2006) In vivo MRI of cancer cell fate at the single-cell level in a mouse model of breast cancer metastasis to the brain. *Magn Reson Med* 56:1001–1010.
18. Hoyte LC, et al. (2010) Molecular magnetic resonance imaging of acute vascular cell adhesion molecule-1 expression in a mouse model of cerebral ischemia. *J Cereb Blood Flow Metab* 30:1178–1187.
19. McAteer MA, et al. (2007) In vivo magnetic resonance imaging of acute brain inflammation using microparticles of iron oxide. *Nat Med* 13:1253–1258.
20. Serres S, et al. (2009) Systemic inflammatory response reactivates immune-mediated lesions in rat brain. *J Neurosci* 29:4820–4828.
21. van Kasteren SI, et al. (2009) Glyconanoparticles allow pre-symptomatic in vivo imaging of brain disease. *Proc Natl Acad Sci USA* 106:18–23.
22. von zur Muhlen C, et al. (2008) MRI-invisible pathology in murine cerebral malaria revealed by a novel contrast agent recognising activated platelets. *J Clin Invest* 118: 1198–1207.
23. Serres S, et al. (2011) VCAM-1-targeted magnetic resonance imaging reveals subclinical disease in a mouse model of multiple sclerosis. *FASEB J* 25:4415–4422.
24. Akhtar AM, et al. (2010) In vivo quantification of VCAM-1 expression in renal ischemia reperfusion injury using non-invasive magnetic resonance molecular imaging. *PLoS One* 5:e12800.
25. McAteer MA, et al. (2008) Magnetic resonance imaging of endothelial adhesion molecules in mouse atherosclerosis using dual-targeted microparticles of iron oxide. *Arterioscler Thromb Vasc Biol* 28:77–83.
26. Haddad O, Chotard-Ghodsnia R, Verdier C, Duperray A (2010) Tumor cell/endothelial cell tight contact upregulates endothelial adhesion molecule expression mediated by NFkappaB: Differential role of the shear stress. *Exp Cell Res* 316:615–626.
27. Salado C, et al. (2011) Resveratrol prevents inflammation-dependent hepatic melanoma metastasis by inhibiting the secretion and effects of interleukin-18. *J Transl Med*, 10.1186/1479-5876-9-59.
28. Tomita Y, et al. (1995) Possible significance of VLA-4 (alpha 4 beta 1) for hematogenous metastasis of renal-cell cancer. *Int J Cancer* 60:753–758.
29. Jantscheff P, et al. (2011) Lysophosphatidylcholine pretreatment reduces VLA-4 and P-Selectin-mediated b16.f10 melanoma cell adhesion in vitro and inhibits metastasis-like lung invasion in vivo. *Mol Cancer Ther* 10:186–197.
30. Bao L, Pigott R, Matsumura Y, Baban D, Tarin D (1993) Correlation of VLA-4 integrin expression with metastatic potential in various human tumour cell lines. *Differentiation* 52:239–246.
31. Läubli H, Borsig L (2010) Selectins promote tumor metastasis. *Semin Cancer Biol* 20: 169–177.
32. Langley RR, et al. (2001) Endothelial expression of vascular cell adhesion molecule-1 correlates with metastatic pattern in spontaneous melanoma. *Microcirculation* 8: 335–345.
33. Nomoto Y, Miyamoto T, Yamaguchi Y (1994) Brain metastasis of small cell lung carcinoma: Comparison of Gd-DTPA enhanced magnetic resonance imaging and enhanced computerized tomography. *Jpn J Clin Oncol* 24:258–262.
34. Katakami N, et al. (2011) Magnetic resonance evaluation of brain metastases from systemic malignances with two doses of gadobutrol 1.0 m compared with gadoteridol: A multicenter, phase II/III study in patients with known or suspected brain metastases. *Invest Radiol* 46:411–418.
35. Grabner G, et al. (2012) Longitudinal brain imaging of five malignant glioma patients treated with bevacizumab using susceptibility-weighted magnetic resonance imaging at 7 T. *Magn Reson Imaging* 30:139–147.
36. Miller KL, Jezzard P (2008) Modeling SSFP functional MRI contrast in the brain. *Magn Reson Med* 60:661–673.
37. Shapiro EM, et al. (2004) MRI detection of single particles for cellular imaging. *Proc Natl Acad Sci USA* 101:10901–10906.
38. Carman CV, Springer TA (2004) A transmigratory cup in leukocyte diapedesis both through individual vascular endothelial cells and between them. *J Cell Biol* 167: 377–388.
39. Dósa E, et al. (2011) MRI using ferumoxytol improves the visualization of central nervous system vascular malformations. *Stroke* 42:1581–1588.
40. Heesakkers RA, et al. (2009) Prostate cancer: Detection of lymph node metastases outside the routine surgical area with ferumoxtran-10-enhanced MR imaging. *Radiology* 251:408–414.
41. Chen HH, et al. (2005) MR imaging of biodegradable polymeric microparticles: A potential method of monitoring local drug delivery. *Magn Reson Med* 53:614–620.
42. McLachlan SJ, et al. (1994) Phase I clinical evaluation of a new iron oxide MR contrast agent. *J Magn Reson Imaging* 4:301–307.
43. Reynolds PR, et al. (2006) Detection of vascular expression of E-selectin in vivo with MR imaging. *Radiology* 241:469–476.
44. von Zur Muhlen C, et al. (2008) Functionalized magnetic resonance contrast agent selectively binds to glycoprotein IIb/IIIa on activated human platelets under flow conditions and is detectable at clinically relevant field strengths. *Mol Imaging* 7: 59–67.
45. Aslakson CJ, Miller FR (1992) Selective events in the metastatic process defined by analysis of the sequential dissemination of subpopulations of a mouse mammary tumor. *Cancer Res* 52:1399–1405.
46. Yoneda T, Williams PJ, Hiraga T, Niewolna M, Nishimura R (2001) A bone-seeking clone exhibits different biological properties from the MDA-MB-231 parental human breast cancer cells and a brain-seeking clone in vivo and in vitro. *J Bone Miner Res* 16: 1486–1495.